Geologie en Mijnbouw **76:** 217–226, 1997.

Quantitative analysis of top-seal capacity: offshore Netherlands, southern North Sea

David R. Spain[1] & Curtis P. Conrad[2]
[1] *Amoco Exploration and Production Technology Group, P.O. Box 3385, Tulsa, Oklahoma, USA;* [2] *Amoco Netherlands B.V., The Hague, the Netherlands*

Received 1 October 1996; accepted in revised form 27 May 1997

Key words: hydrocarbon exploration, Triassic, Main Buntsandstein, petrophysics, capillary pressure, caprock

Abstract

Sealing characteristics of the caprock to the Main Buntsandstein reservoir sands in the P blocks in the Dutch offshore are assessed based on a core from the P15 well. The core which represents the Main Buntsandstein, Solling, Röt, and Muschelkalk interval has been analyzed using standard geologic and petrophysical techniques including mercury-injection capillary-pressure tests. The caprock to the Main Buntsandstein reservoir sands consists of anhydritic and/or dolomitic sandstone to argillaceous siltstone, silty shale, and dolostone. Early emplacement of nodular anhydrite followed by cementation and replacement by anhydrite, dolomite, and siderite has resulted in tight, submicroporous pore geometries which act as good to excellent seals. Capillary entry pressures of the best caprock lithologies are such that gas columns of the order of 300 m could potentially be trapped. The actual column height in P15 is about 125 m as indicated by RFT data. The presence of significant gas accumulations in the Main Buntsandstein in the P12, P14, P15, P18 and adjoining Q8 and Q16 blocks suggests that the P15 top-seal quality may be representative for that area.

Introduction

The P and Q Blocks cover about 12 000 km^2 of the southern Dutch North Sea (Figure 1). Drilling for gas-bearing sandstones of Early Triassic age in the offshore Netherlands sector of the North Sea began in late 1987 by Amoco Netherlands B.V. Successful exploration wells in the P12, P14, P15, P18, Q8 and Q16 blocks have defined a productive fairway in the Main Buntsandstein reservoirs. Exploitation of the offshore blocks P15 and P18 began in early 1991. A total of ten consecutive successful Main Buntsandstein wells has resulted in proven reserves of over 25.5 billion (10^9) cubic meters of gas (900 BCFG: billion cubic feet of gas). These wells have tested at rates between 0.71 and 1.42 million cubic meters (25 and 50 million cubic feet) of gas per day. The P15-14 well, hereafter called the P15 well, was drilled to a total depth of about 3500 m (11 000 ft). The well location is approximately 40 km (25 miles) west of The Hague in 30 m (90 ft) of water (Figure 1). The P15 field was developed in conjunction with other gas discoveries made by Amoco and its partners in the P15 and P18 blocks. Production began in October 1993 from a facility with a total capacity of about 14.16 million cubic meters (500 million cubic feet) of gas per day. Amoco Netherlands is a 29.9% license owner and operator in the P15c license.

Detailed integration of depositional-facies interpretations from a conventional core with proprietary petrographic, isotopic, fluid-inclusion, depth-of-burial, and pressure studies have been used previously to explain diagenesis and fluid distribution within the Main Buntsandstein sandstone reservoirs. Structural mapping of 3-D seismic over blocks P15 and P18 is currently being used to define discovered structures and to delineate new drillable prospects. To date, however, no studies have been made of the rock overlying the reservoir unit; consequently, knowledge of the true top seal is limited. Because the technical risk associated with seals in drillable prospects is high due to the poorly understood effects of both local and regional unconformities, a 35.5 m core was cut in the Amoco P15

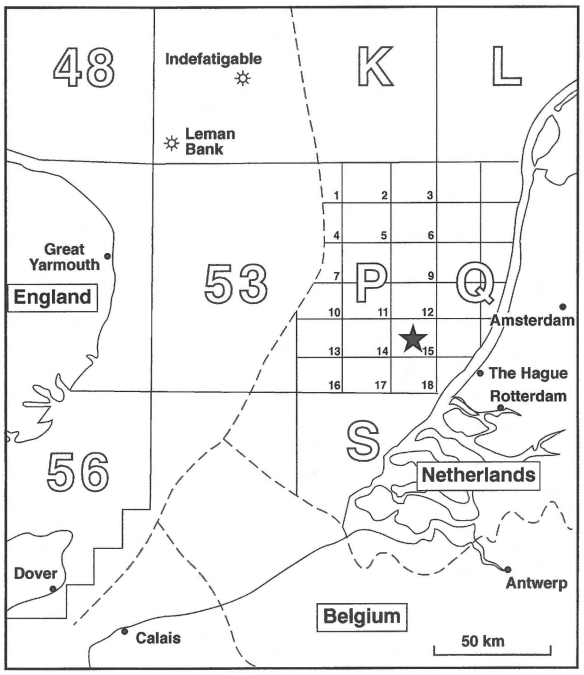

Figure 1. Location map of study area. The P15 well is approximately 40 km (25 miles) west of the Hague in 30 m (90 ft) of water

well (3117.0–3152.5 m core depth) for top-seal analysis. In the P15 well (Figure 2), the Main Buntsandstein is topped by a local disconformity, the Hardegsen Unconformity (Figure 3). Overlying the disconformity are the Solling, Röt, and Muschelkalk Formations, a lithologically mixed package of limestones, siltstones, shaly sandstones, dolomitic shales and evaporitic mudstones. In adjacent, undrilled prospects, however, the Muschelkalk, Röt and Solling Formations are partially removed at a regional, basal Cretaceous unconformity, the Hils Unconformity. Therefore, a factual knowledge of the specific sealing unit(s), their capacity and/or integrity, and the likelihood of their absence at the Hils Unconformity will help answer questions about seal risk. In addition, seal-capacity data will help resolve important data discrepancies among seismic velocity and structural closure, net pay, and 'apparent' gas-water contacts in well logs and pressure data.

Lithofacies and environments of deposition

Overall, the lithology of the cored interval ranges from dolomitic and/or anhydritic sandstone in the Main Buntsandstein to highly variable anhydritic and/or dolomitic sandstone to argillaceous siltstone, silty shale, and rarely dolostone in the Solling, Röt, and Muschelkalk Formations. All of these rocks contain variable amounts of nodular anhydrite.

Four distinct lithofacies were defined on the basis of lithology, texture, and sedimentary structures. The four lithofacies are: 1) dolomitic and/or anhydritic, fine- to coarse-grained sandstone; 2) thinly interbedded and/or interlaminated shale and argillaceous, very fine-grained sandstone to siltstone; 3) thinly interbedded, argillaceous, anhydritic and/or dolomitic, very fine- to fine-grained sandstone; anhydritic, argillaceous siltstone; and silty shale; and 4) fining-upward anhydritic, dolomitic, medium- to very fine-grained sandstone.

The entire sequence is interpreted to contain depositional features characteristic of a desert environmental system. Eolian dune and interdune deposits are erosively overlain by a thick sequence of inland sabkha deposits containing localized intermittent stream or wadi, and intermittent desert lake or pond deposits. The lack of evidence for marine organisms and the general paucity of biogenic activity suggest an inland setting rather than a coastal sabkha and dune setting. The abundance of dolomitic matrix suggests that the system may, however, be representative of the more landward portion of a coastal system, far enough inland to account for a lack of algal growth, bioturbation, and marine-derived grains.

Lithofacies 1: Dolomitic and/or anhydritic, fine- to coarse-grained sandstone (eolian dune to interdune)

Eolian dune sandstones in this lithofacies are commonly dolomitic and occasionally argillaceous or anhydritic. Compositionally, they are subarkosic arenites which grade locally into lithic, subarkosic arenites and quartz arenite. Bedding is variable in this lithofacies; the lower portion of the cored interval (3146.55–3152.5 m) is distinctly bedded, containing low- to high-angle, planar cross-stratification with localized slightly wavy bedding and shaly laminations (Figure 4). The cross-bedded sandstones generally have a bimodal grain-size distribution containing subrounded to subangular fine-grained sand and mostly well-rounded medium- to coarse-grained sand. The two size fractions can be intermixed or segregated into alternating laminae. The laminae locally appear to contain both normal and inverse grading. Erosional or truncated surfaces are common and burrowing or rooting appears to have disrupted the wavy, shaly laminations. Adhesion ripples

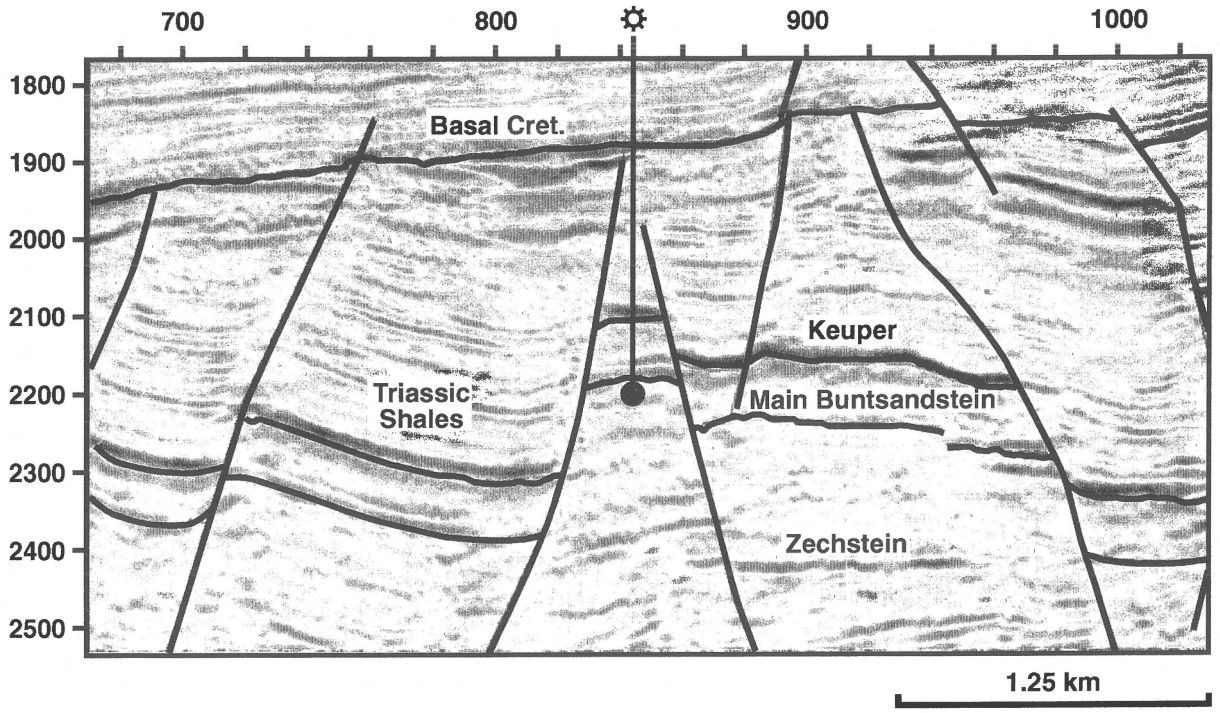

Figure 2. Seismic line 520 showing location of P15 gas discovery in Main Buntsandstein (Lower Triassic). Strong reflector overlying sealing unit is caused by anhydrite in Upper Triassic Keuper Formation. Verticale scale: two-way travel time, milliseconds

are also associated with the wavy-bedded portions of the unit.

The upper portion of this lithofacies is less distinctly bedded and appears homogeneous, although the bedding is locally disrupted by burrowing. The apparent homogeneity is partly due to a much more uniform fine-to-medium sand grain-size distribution, which results in a higher degree of sorting. These upper sandstones vary from tightly cemented to very friable. Diagenetic contacts frequently occur within this unit, and possibly represent paleowater tables. These boundaries are irregular, cut across bedding, and are defined by localized concentrations of dolomite and anhydrite cement, and fine- to coarse-crystalline pyrite. The top of the unit appears to be an erosional surface and contains abundant cement-filled fractures, small-scale faults, and breccia which has been infilled by detrital clay. This upper zone may represent a depositional hiatus or disconformity.

Lithofacies 2: Thinly interbedded and/or interlaminated shale and argillaceous, very fine-grained sandstone to siltstone (lacustrine or intermittent lake)

Laminated dark-gray shales with thin interbeds of rippled, argillaceous siltstone and very fine-grained sandstone are interpreted to represent deposition in a lacustrine or intermittent lake environment (Figure 5). Burrows and apparent mudcracks (suggesting intermittent desiccation) have disrupted laminae and the siltstone and sandstone beds locally display soft-sediment deformation and contain some shale rip-up clasts, suggesting deposition by higher-energy fluvial or eolian processes. Shale beds contain planar to slightly wavy laminations that commonly contain thin silt laminae and carbonaceous debris that is concentrated along bedding. The matrix is predominantly clay with relatively minor amounts of fine-crystalline dolomite. Siltstone and sandstone laminae contain an argillaceous matrix with locally common 'patches' of siderite and anhydrite.

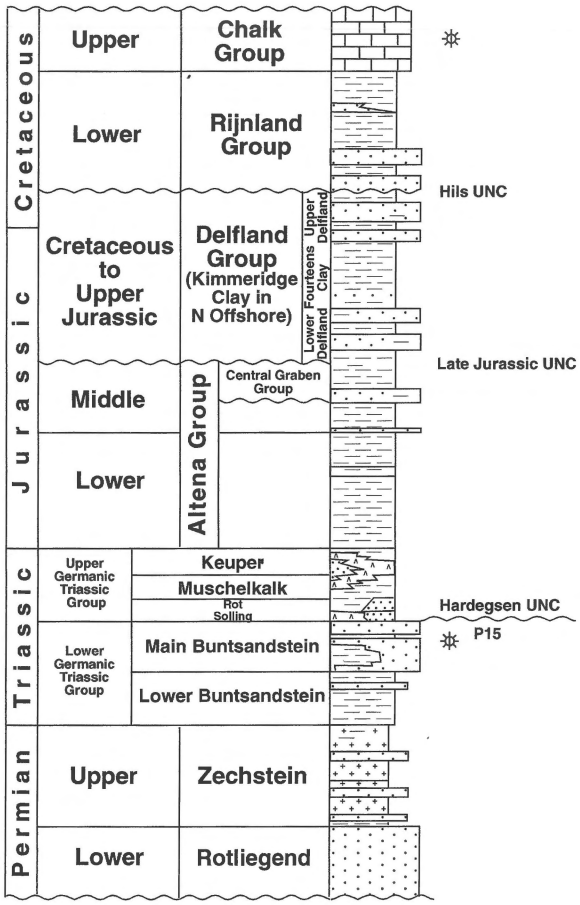

Figure 3. Stratigraphic relationships in P15 area. Hardegsen Unconformity separates the seal from the reservoir.

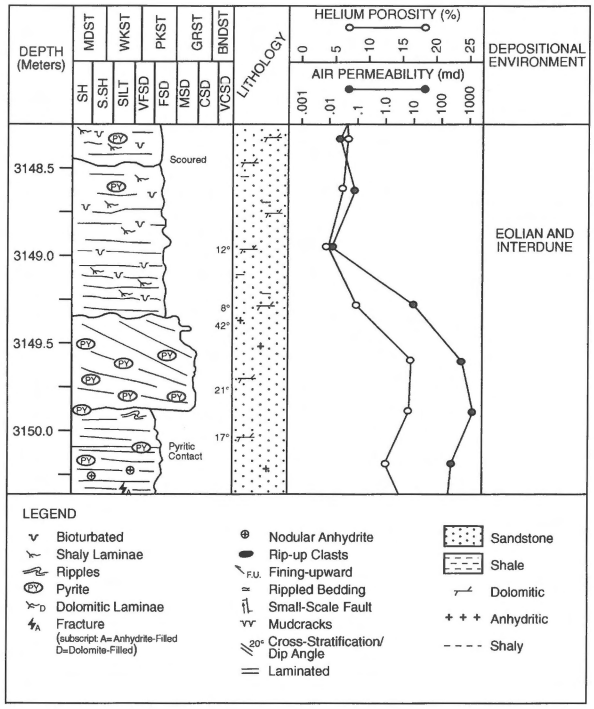

Figure 4. Lithofacies 1. The dolomitic and/or anhydritic, fine- to coarse-grained sandstone comprises the principal reservoir facies in the Main Buntsandstein in the P15 well. Legend also applies to Figures 5 to 7.

Lithofacies 3: Thinly interbedded argillaceous, anhydritic and/or dolomitic, very fine- to fine-grained sandstone, anhydritic, argillaceous siltstone, and silty shale (inland sabkha)

The thinly interbedded, very fine- to fine-grained sandstones, siltstones and shales of Lithofacies 3 are interpreted as inland sabkha deposits (Figure 6). The rocks in this lithofacies are highly variable in lithology and mineralogy. Most of them are poorly sorted, with occasionally moderately to well-sorted beds. The very fine-grained sandstones and siltstones are slightly argillaceous and can be classified as subarkosic arenites. Most of the sandstones are silty, dolomitic and/or anhydritic. Framework grains are largely monocrystalline quartz with rape to sparse amounts of polycrystalline quartz, chert, potassium feldspar, and rock fragments. The rock fragments are predominantly shale and dolo-

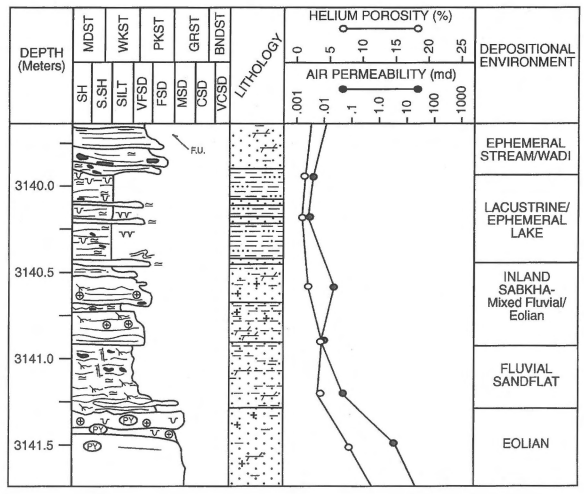

Figure 5. Lithofacies 2. The thinly interbedded and/or interlaminated shale and argillaceous, very fine-grained sandstone to siltstone comprise the seal facies, which disconformably overlies the reservoir facies. Legend in Figure 4.

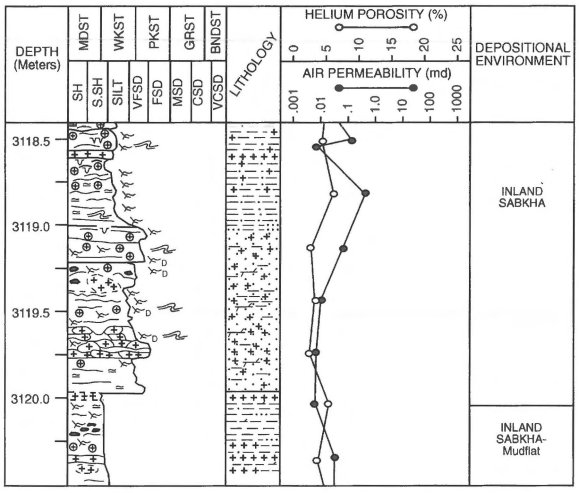

Figure 6. Lithofacies 3. These thinly interbedded, very fine- to fine-grained sandstones, siltstones, and shales are interpreted as inland sabkha deposits. Note abundance of displacive, early anhydrite nodules. Legend in Figure 4.

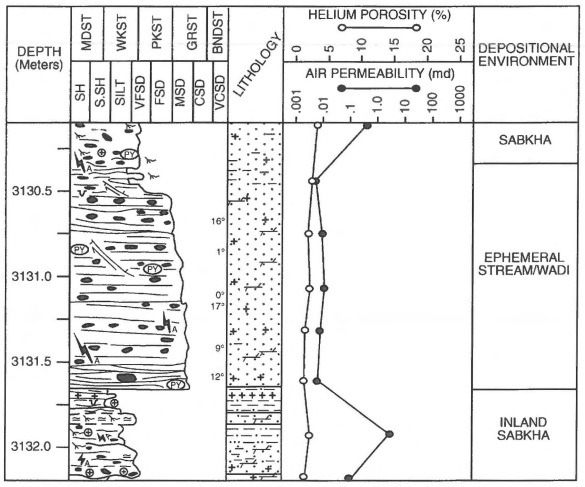

Figure 7. Lithofacies 4. Medium- to very fine-grained sandstones generally fine upward, yet abundant dolomite and anhydrite cement and localized pyrite greatly reduce porosity and permeability. Legend in Figure 4.

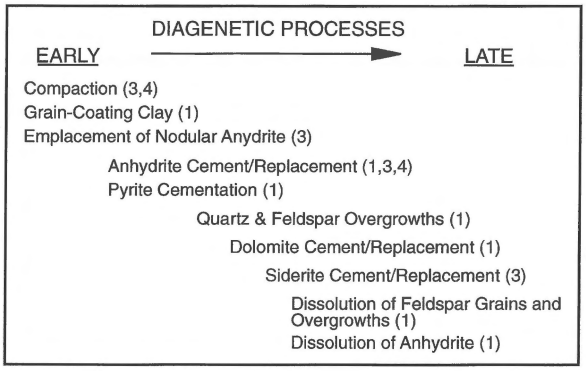

Figure 8. Diagenetic history of cored interval of well P15. Early compaction and emplacement of anhydrite nodules and cement are the primary mechanisms of seal formation. Numbers in parentheses refer to lithofacies which are most affected by given diagenetic process.

mudstone rip-up clasts that are rounded to tabular in shape. Metamorphic (schistose) rock fragments are also present.

Much of the coarser sediment in this lithofacies appears to have been deposited by fluvial processes of varying flow regimes. The bedding is highly variable and includes horizontal laminations, low-angle cross-stratification, rippled beds, and wavy bedding. Common graded bedding and scoured surfaces suggest fluvial transport. A few zones, however, contain low-angle, planar-bedded sandstones that are well-sorted and may represent eolian transport during dry periods.

Shaly laminae to thin beds are common in all rock types and often contain mudcracks or are partially eroded. Less common dolomitic laminae exhibit similar features. As a result of the erosion of the shale and dolomite laminae, tabular to rounded rip-up clasts are common. Shales are silty and/or sandy, dolomitic, and occasionally anhydritic. The matrix is largely detrital clay with much lesser amounts of fine-crystalline dolomite.

All of the rock types can contain significant amounts of clay, anhydrite, and or dolomite. Alteration of gypsum and emplacement of displacive anhydrite nodules has greatly altered the appearance of these rocks. These anhydrite nodules are of varied size and shape, and can occur as isolated nodules or in clusters. Their emplacement has generated soft-sediment deformation, resulting in deformed bedding and small-scale faulting. The anhydrite occasionally has a contorted or diapiric form. The anhydrite nodules and mudcracks indicate an arid to semi-arid environment that was intermittently wet and desiccated.

Lithofacies 4: Fining-upward anhydritic, dolomitic, medium- to very fine-grained sandstone (intermittent stream or wadi)

These medium- to very fine-grained sandstones generally fine upward and contain common dolomite and anhydrite cement and localized pyrite (Figure 7). The

units have erosional lower contacts, commonly contain shale and dolomite rip-up clasts, and frequently exhibit truncation surfaces in their lower portions. The bedding is mostly low- to medium-angle cross-stratification that appears trough-bedded in the lower portion of the units. The medium-grained sandstones are compositionally similar to sandstones in the other lithofacies, but contain a higher proportion of sedimentary and metamorphic rock fragments. The depositional units observed in the core are relatively thin, suggesting that the intermittent stream channels were fairly shallow and that the channels may have regularly shifted position through time.

Diagenetic history and mechanisms of seal formation

The diagenetic history is variable for the reservoir sandstones and seal rocks in the cored interval (Figure 8). The Lithofacies 1 sandstones of the Main Buntsandstein were most affected by dolomite cementation and, to a lesser extent, by anhydrite cementation. Where these cements are well-developed, the porosity is limited to minor amounts of secondary intergranular pore space. Localized dissolution of anhydrite cement has served to create the best reservoir quality. The degree of intergranular cementation is the major control on overall reservoir quality in these sandstones. This cementation was affected by several factors, namely: i) the emplacement of early anhydrite cement which prevented severe compaction; ii) detrital illitic grain-coating clays which inhibited subsequent quartz and feldspar overgrowths; iii) pore-filling and replacement by pyrite, dolomite, and siderite cement; iv) dissolution of feldspar grains in poorly cemented sandstones; and v) the dissolution of anhydrite cement and replacement anhydrite.

In contrast to reservoir-quality lithofacies in the Main Buntsandstein, rocks in the Solling, Röt and Muschelkalk Formations contain high amounts of depositional matrix and early emplaced nodular anhydrite, and are excellent seals. Anhydrite, dolomite, pyrite, and siderite have commonly replaced matrix and framework grains and filled virtually all former intergranular pores in the matrix-poor sandstones. Rocks containing the highest proportions of lithic fragments, specifically shale and dolomudstone rip-up clasts, have been affected by early compaction. Very fine-grained sandstones exhibit relatively low levels of compaction largely due to the emplacement of early coarse-crystalline to poikilitic anhydrite. The anhydrite occurs as both an intergranular cement and as a replacement of framework grains and matrix.

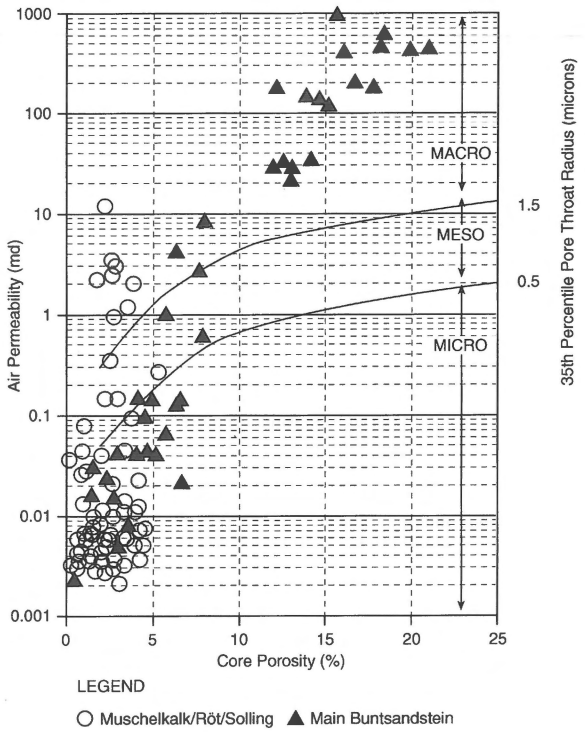

Figure 9. Porosity-permeability crossplot for the P15 core. Note occurrence of seal-quality samples in Main Buntsandstein Formation. Pore-throat radius contours are based on empirical relationships among porosity, permeability and pore-throat size from mercury-injection capillary-pressure data.

Anhydrite occurs as single nodules or as aggregates of nodules throughout the Solling, Röt and Muschelkalk Formations. The extensive soft-sediment deformation observed in the core resulted from early crystallization of the displacive anhydrite nodules, prior to significant lithification of the surrounding sediment. The occurrence of nodular anhydrite is the primary agent of pore-volume reduction and seal formation in the cored interval.

Coarse- to medium-crystalline pyrite cement has also filled intergranular pores and partially replaced framework grains. Pyrite is also present as a replacement of matrix and organic matter. Textural relationships also suggest that medium-to coarse-crystalline dolomite cement has replaced anhydrite cement, framework grains, and matrix. Fine- to medium-crystalline siderite cement and replacement siderite have also reduced pore volume and assisted seal formation.

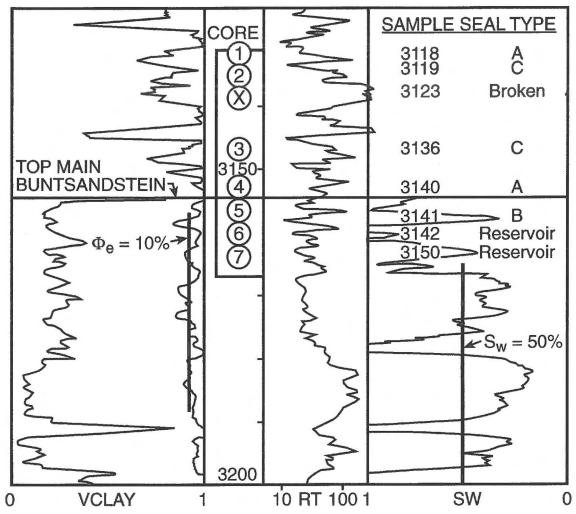

Figure 10. Interpreted well log in well P15, showing core interval and mercury-injection sample depths. Note that core and sample depths (3117–3152.5 m) are 6 m deeper than well-log depths. VCLAY = volume of clay from normalized gamma-ray log, RT = formation resistivity from induction log, Sw = calculated formation water saturation, Φ_e = calculated effective porosity. Sample numbers 1–7 refer to Figure 11.

Petrophysical analysis of seal integrity and capacity

Conventional core analysis

Radiographic features observed in the P15 core were extremely useful in analyzing the seal integrity of the Solling, Röt, and Muschelkalk Formations. Although the unslabbed core appeared to be highly fractured and rubbled, detailed examination of X-ray video fluoroscan, coupled with visual examination of the slabbed core, revealed that most, if not all, of these features were induced during the coring process.

The abundance of localized anhydrite mineralization and nodular anhydrite supports the interpretation of the diagenetic history of the cored interval as observed from petrologic and petrographic thin-section analysis. Pore-filling and replacement cementation by anhydrite has greatly contributed to the overall seal quality of the interval. The lack of open, natural fractures and the abundance of fully mineralized gouge zones and fractures support the conclusion that loss of seal integrity through mechanical breakage is unlikely.

Conventional core analysis of the Solling, Röt, and Muschelkalk Formations reflects the heterogeneity in pore geometries. These tests included air-permeability, helium-porosity, and grain-density measurements. A crossplot of air permeabilities and helium porosities is shown in Figure 9. Porosities range from 0.70 to 5.4%, and vertical permeabilities from 0.002 to 0.240 md. Grain densities range from 2.71 to 2.92 g/cm^3, reflecting the wide variation of mineralogy and the abundance of anhydrite and pyrite in the samples.

When a plot of isopore-throat radii, as calculated using the technique of Winland (in Pittman 1992), is overlain on the porosity-permeability crossplot (Figure 9), it is apparent that the majority of samples from the Solling, Röt, and Muschelkalk intervals exhibit micro- to submicroporous pore geometries. Several points from the Main Buntsandstein also fall in the microporous category; these samples, from the upper part of the Main Buntsandstein 'reservoir', exhibit excellent sealing characteristics.

Quantitative analysis of seal capacity

Hydrocarbons will be trapped if the differential buoyancy pressure at all points in the reservoir is less than the capillary displacement pressure of the reservoir boundary material (Sneider 1991). Capillary properties of rocks are usually measured in the laboratory by injecting mercury into dry rock samples, although other capillary-pressure measurement techniques are available. Mercury is forced into a rock sample at incrementally increasing pressures until a predetermined value is reached. A plot of mercury pressure versus volume of mercury injected (expressed as a percentage of pore volume) is referred to as a mercury-injection capillary-pressure curve. The displacement pressure (Pd) can be determined from the laboratory-derived mercury-air capillary-pressure curve, once corrections for subsurface gas and water, or oil and water reservoir systems have been made.

The magnitude of the resistance force is a function of the hydrocarbon-water interfacial tension, wettability, and geometry of the pore throats of the rock. The capillary displacement pressure is that force required to displace water from a pore and is analogous to injection pressure in the mercury-injection technique. If the displacement pressure for any hydrocarbon-water-rock system can be determined at the sealing interface, then the maximum hydrocarbon-column height necessary to migrate hydrocarbons through the seal can be determined (Schowalter 1979). The displacement pressure therefore determines the sealing capacity for capillary seals.

High-pressure (0–30 000 psi) mercury-injection capillary-pressure tests were performed on 'representative' seal lithologies after screening standard core-analysis data (Figure 10). These date were reviewed for quality and the laboratory displacement pressures were converted to subsurface gas-water displacement pressures; the subsurface gas-water displacement pressures were then converted to a gas-column height which can be sealed by the representative sample. Details of these conversions are as follows:

1) Convert laboratory mercury-injection displacement pressure (Pd_{lab}) to subsurface gas-water displacement pressure (Pd_{res}):

$$Pd_{res} = \left[Pd_{lab} \frac{(\gamma cos\theta)_{res}}{(\gamma cos\theta)_{lab}} \right]$$

where:

γ_{res} = gas-water interfacial tension (= 25 dynes/cm) corrected for subsurface pressure (33.4 MPa) and temperature (106 °C),
θ_{res} = gas-water contact angle (assume water-wet reservoir) = 0°,
γ_{lab} = mercury-air interfacial tension = 484 dynes/cm,
θ_{lab} = mercury-air contact angle = 140°.

2) Convert subsurface gas-water displacement pressure (Pd_{res}) to hydrocarbon-column height (H) in meters:

$$H_{(m)} = \left[\frac{Pd_{res}}{(0.433)(\rho_w - \rho_g)} \right] \times 0.305$$

where:

ρ_w = subsurface water density = 1.067 g/cm^3,
ρ_g = subsurface gas density = 0.259 g/cm^3,
0.433 = units conversion (g/cm^3 to psi/ft: pounds per square inch per foot),
0.305 = units conversion (feet to meters).

Note that in these calculations, subsurface water and gas densities were derived from RFT pressure measurements in the P15 well. Table 1 documents the results of the analysis. Figure 11 shows the actual data used.

In order to facilitate communication regarding the seal quality and capacity of the Solling, Röt, and Muschelkalk samples, a seal-classification scheme similar to that of Sneider (1991) was derived using actual fluid densities at subsurface pressure and temperature conditions (Table 2). Laboratory mercury-air displacement pressures which correspond to the arbitrarily chosen seal-quality or-column-height classification are also shown in Figure 11.

Table 1. High-pressure mercury-injection capillary-pressure test results and calculated gas-column heights for Amoco Netherlands well P15.

Depth (m)	Phi (%)	Ka (md)	$Pd_{(lab)}$ (psi)	$Pd_{(res)}$ (psi)	H (m)
3118	4.2	0.0043	20 000	1306	1189
3119	1.3	0.0051	800	54	48
3136	1.5	0.0165	2 000	136	119
3140	2.5	0.0022	10 000	680	594
3141	4.1	0.0044	2 800	190	166
3142	6.0	1.89	11	0.75	—
3150	15.4	8.59	10	0.68	—

Phi = porosity, Ka = air permeability, $Pd_{(lab)}$ = laboratory displacement pressure, $Pd_{(res)}$ = reservoir displacement pressure, H = gas column height, psi = pounds per square inch; 1 psi = 6.894 757 kPa.

Table 2. Seal classification system, Amoco Netherlands well P15. After Sneider (1991).

Seal type	Gas column held	
A	> 300 m	(> 1000 ft)
B	150 m but < 300 m	(500 ft but < 1000 ft)
C	30 m but < 150 m	(100 ft but < 500 ft)
D	15 m but < 30 m	(50 ft but < 100 ft)
E	< 15 m	(< 50 ft)

Assumes: Water density = 1.067 g/cm^3 (0.462 psi/ft), Gas density = 0.259 g/cm^3 (0.112 psi/ft), Pressure = 33.37 MPa (4840 psi), Temperature = 106 °C (223°F).

The relative stratigraphic positions of the various seal lithologies are important with respect to the Hils Unconformity contact. Type A seals (capable of holding >300 m of gas column) occur directly above the reservoir in the Solling Claystone. Specifically, the core sample from 3140 m depth (Lithofacies 2) exhibits a gas-water displacement pressure of 680 psi; an equivalent gas-column height of 594 m would be required to displace water from the seal's pore system.

Additionally, multiple, stacked capillary seals within the Solling, Röt, and Muschelkalk Formations greatly increase the thickness of the overlying effective sealing unit and greatly reduce the risk of lateral discontinuity and loss of seal integrity by fracturing.

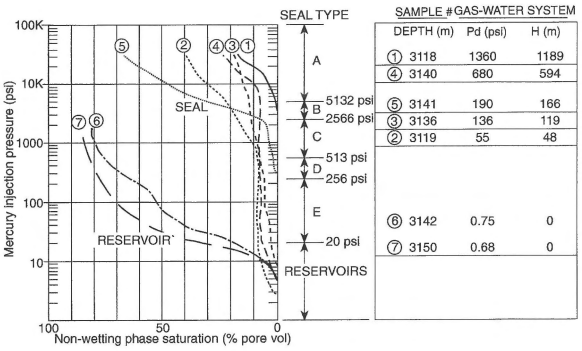

Figure 11. High-pressure mercury-injection test results for the P15 core. See Figure 10 for sample positions and Table 2 for seal classification. Note that sample from 3123 m fractured during analysis and is not included here. Samples 1–5 are seal rocks, samples 6 and 7 are reservoir rocks. Pd = displacement pressure, H = column height.

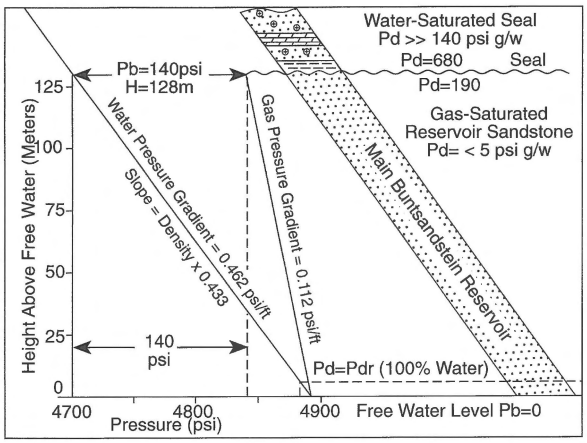

Figure 12. RFT (Repeat Formation Test) gradients, Amoco Netherlands well P15. RFT data agree well with seal capacity calculated from mercury-injection capillary-pressure data. The RFT data indicate a gas column height of about 128 m. Pb = buoyancy pressure due to gas-water density difference over column height. Pdr = capillary displacement pressure of reservoir, Pd = capillary displacement pressure, g/w = gas/water.

RFT pressure data

Repeat Formation Tester (RFT) pressure data from the well P15 document a well-defined gas gradient (0.112 psi/ft). When plotted in combination with RFT pressures obtained from water-bearing reservoirs (aquifers) in nearby wells, the intersection of the two gradients defines a free-water level (zero buoyancy pressure) or 'gas-water contact' in the well. The vertical distance between the shallowest pressure point (top Main Buntsandstein) and the free-water level defines the vertical gas-column height in the reservoir. At the top of the gas column, the difference in gas and water pressure gradients defines the maximum buoyancy pressure in the trapped accumulation (Figure 12). The buoyancy pressure at the crest of the structure will be equal to or less than the capillary displacement pressure of the seal rock.

All Type A and Type B seals meet these column-height requirements in the P15 well. In fact, the Type A seal, which immediately overlies the reservoir unit, exhibits a gas-water capillary displacement pressure of 680 psi. The excess capillary pressure, 540 psi over the buoyant force of 140 psi, represents an additional 472 m of gas column which can be sealed in the structure. The RFT pressure data are in good agreement with data derived from mercury injection tests. These data provide a quantitative check against seal-capacity and gas-column-height calculations.

Conclusions

1. The true top seal for the P15 hydrocarbon accumulation is provided by thinly interbedded and interlaminated shale and argillaceous, very fine-grained sandstone to siltstone which directly overlie the reservoir unit. This lithofacies contains Type A seals which are capable of supporting gas-column heights in excess of 300 m. Interlaminated shales in this lithofacies are interpreted to represent deposition in a desert lacustrine environment; interbedded siltstone and sandstone beds reflect higher-energy eolian or fluvial processes.
2. Early emplacement of nodular anhydrite, followed by cementation and replacement by anhydrite, dolomite, and siderite has formed a tight, submicroporous pore geometry in all of the seal lithologies observed. Late-diagenetic processes (quartz and feldspar overgrowth formation, pore-filling pyrite cementation, dissolution of anhydrite and feldspar are mostly restricted to reservoir sandstones.
3. The effectiveness of the top seal is dependent on the lateral continuity of the rock types and their associated petrophysical characteristics, as well as the mechanical integrity of the overlying seal unit. The early-diagenetic processes which are responsible for seal formation are closely associated with the depositional environments and the paleoclimatic conditions associated with them.
4. Loss of seal integrity through mechanical deformation does not appear to be a problem. Detailed

X-ray video fluoroscan of the P15 core reveals a lack of open, natural fractures and an abundance of fully mineralized gouge zones and microfaults, suggesting that loss of seal integrity through rupture is unlikely.

5. RFT pressure data are in good agreement with data derived from mercury injection tests. Although Type A seals capable of containing over 1000 m of gas column are present in the core, the Type A seal which disconformably overlies the reservoir unit exhibits a subsurface gas water capillary displacement pressure of 680 psi. The excess capillary pressure, 540 psi over the buoyant force of 140 psi exerted by the P15 gas column, represents an additional 472 m of gas column which can be sealed in the P15 structure.

Acknowledgements

The authors wish to thank the Amoco Exploration and Production Technology Group, Amoco Netherlands B.V. and its partners, Veba Oil Nederland B.V., Dyas B.V., Oranje Nassau Energie B.V., Clyde Petroleum Exploratie B.V., DSM Energie B.V., Energie Beheer Nederland B.V., and Van Dyke Netherlands, Inc. for permission to publish this work. Special thanks are given to Peter F. Purrazella for his excellent petrographic and sedimentologic descriptions. Routine and special core analyses were performed by K&A Energy Consultants. Julie Youngblood and Moira Hathcock are thanked for their diligence and patience in manuscript preparation and revision. Finally, much appreciation is expressed to Bernie Leclerc, Hans Klasen, J.A. Mulock Houwer, Dick A.J. Batjes, and an anonymous reviewer for their constructive help in reviewing the manuscript.

References

Pittman, E.D. 1992 Relationship of porosity and permeability to various parameters derived from mercury injection-capillary pressure curves for sandstone – Amer. Assoc. Petroleum Geol. Bull 76: 191–198

Schowalter, T.T. 1979 Mechanics of secondary hydrocarbon migration and entrapment – Amer. Assoc. Petroleum Geol. Bull. 63: 723–760

Sneider, R.M. 1991 Evaluation of reservoirs and seals – Amer. Assoc. Petroleum Geol. Education Dept. Short Course Notes. Midland, TX. 347 pp